ACS APPLIED MATERIALS & INTERFACES

Research Article

www.acsami.org

Large Area, Facile Oxide Nanofabrication via Step-and-Flash Imprint Lithography of Metal–Organic Hybrid Resins

Saman Safari Dinachali,[†,‡] Jarrett Dumond,*[,†] Mohammad S. M. Saifullah,*[,†] Kwadwo Konadu Ansah-Antwi,[†,§] Ramakrishnan Ganesan,[∥] Eng San Thian,[‡] and Chaobin He[†,⊥]

[†]Institute of Materials Research and Engineering, A*STAR (Agency for Science, Technology and Research), 3 Research Link, Singapore 117602, Republic of Singapore

[‡]Department of Mechanical Engineering, National University of Singapore, 9 Engineering Drive 1, Singapore 117576, Republic of Singapore

[§]Department of Electrical and Computer Engineering, National University of Singapore, E4-5-45, 4 Engineering Drive 3, Singapore 117583, Republic of Singapore

[∥]Department of Chemistry, Birla Institute of Technology & Science, Pilani–Hyderabad Campus, Jawahar Nagar, Shameerpet Mandal, Hyderabad 500 078, Andhra Pradesh, India

[⊥]Department of Materials Science & Engineering, National University of Singapore, 21 Lower Kent Ridge Road, Singapore 119077, Republic of Singapore

Supporting Information

ABSTRACT: Step-and-flash imprint lithography (S-FIL) is a wafer-scale, high-resolution nanoimprint technique capable of expansion of nanoscale patterns via serial patterning of imprint fields. While S-FIL patterning of organic resins is well known, patterning of metal–organic resins followed by calcination to form structured oxide films remains relatively unexplored. However, with calcination shrinkage, there is tremendous potential utility in easing accessibility of arbitrary nanostructures at 20 nm resolution and below. However, barriers to commercial adoption exist due to difficulties in formulating polymerizable oxide precursors with good dispensability, long shelf life, and resistance to auto-homopolymerization. Here we propose a solution to these issues in the form of a versatile resin formulation scheme that is applicable to a host of functional oxides (Al_2O_3, HfO_2, TiO_2, ZrO_2, Ta_2O_5, and Nb_2O_5). This scheme utilizes a reaction of metal alkoxides with 2-(methacryloyloxy)ethyl acetoacetate (MAEAA), a polymerizable chelating agent. Formation of these inorganic coordination complexes enables remarkable resistance to auto-homopolymerization, greatly improving dispensability and shelf life, thus enabling full scale-up of this facile nanofabrication approach. Results include successively imprinted fields consisting of 100 nm linewidth gratings. Isothermal calcination of these structures resulted in corresponding shrinkage of 75–80% without loss of mechanical integrity or aspect ratio, resulting in 20 nm linewidth oxide nanostructures.

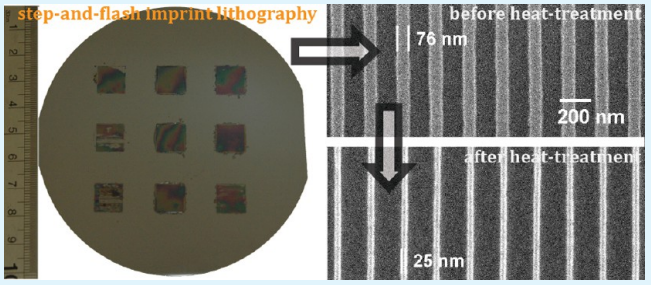

KEYWORDS: *step-and-flash nanoimprint lithography, metal oxides, nanolithography, nanofabrication, metal–organic resins*

INTRODUCTION

Thin film metal oxides, due to their excellent electrical, mechanical, and optical properties and high transparency, continue to be tremendously important for myriad applications, particularly solar cells, sensors, photocatalysts, thin film transistors, transparent electrodes, and other devices.[1−3] Many of these applications require easy access to nanoscale surface structures in oxides over a large area in order to enable device function, enhance performance, or achieve economies of scale. While conventional oxide nanostructuring approaches exist such as optical lithography,[4,5] electron beam lithography,[6−8] and focused ion beam writing,[9] these approaches are indirect and complex in the sense that they rely on multi-step patterning and vacuum etching of a polymer film deposited on top of the target oxide film. In addition, polymer nanostructures formed with these techniques must correspond precisely in dimension with the desired oxide features. Therefore, all challenges associated with top-down fabrication on the nanoscale such as the optical diffraction limit in the case of photolithography and beam scattering issues in the case of electron and focused ion beam writing will apply. In response, UV nanoimprint lithography (UV-NIL) and particularly step-and-flash nanoimprint lithography (S-FIL) have emerged as viable alternatives to the other above-mentioned conventional

Received: September 23, 2013
Accepted: November 26, 2013
Published: November 26, 2013

techniques due to their ability to access the nanoscale without the light diffraction and beam scattering limitations noted above. In addition, these contact lithography approaches retain a favorable combination of simplicity, versatility, low cost, and the potential for achieving high throughput.[10−14] Unfortunately, mold templates used in UV-NIL and S-FIL generally rely upon the above-mentioned conventional lithography techniques for fabrication. Thus, indirectly, the same light diffraction and beam scattering limitations apply to nanoimprinting techniques through mold fabrication as is applicable to conventional lithography. One way of lifting these limitations, in addition to enabling a unique means of nanostructuring oxide films, is to take advantage of the calcination shrinkage inherent to sol−gel processing to easily access the nanoscale from much larger patterned features. For example, it is possible to form 100 nm diameter hybrid metal−organic structures and, with calcination shrinkage, achieve 20 nm equivalent oxide structures of the same aspect ratio, feature density, and pitch. Note that the duty cycle, or surface area coverage of features, is reduced by calcination shrinkage. This can, to a certain extent, be compensated for by increasing the duty cycle of the as-imprinted metal−organic structures and by tuning the degree of calcination shrinkage such that the amount of shrinkage required to achieve the desired resolution in oxide is minimized. However, care must be taken to select end-applications that do not require extremely high density nanostructures for use with this approach.

In any case, by adapting metal−organic materials for use in S-FIL, it is possible to fabricate mold templates with features up to 8 times larger in diameter than the actual desired structures. Such a feat would significantly improve the ease and economics of fabrication, as S-FIL can then be used to expand the coverage area of the calcined oxide nanostructures in step-and-repeat fashion.

In recent years, the importance of organic−inorganic hybrid resins to fabricate nanostructures with inorganic character using NIL has gained considerable attention.[15−23] However, conventional NIL techniques such as UV and thermal NIL rely heavily on a one-step, whole-wafer patterning process, which requires a large and expensive mold to achieve large area patterning. Furthermore, the difficulty in controlling and minimizing defects and achieving good residual layer uniformity increases considerably with increasing imprint field area. S-FIL in contrast can utilize relatively small molds in order to solve both issues of economics and defect control. Furthermore, S-FIL is greatly advantaged over competing nanoimprinting techniques by its employment of drop-on-demand inkjet dispensing in order to fill non-uniform mold cavity distributions while retaining uniform residual layer thicknesses. In addition to easier access to the nanoscale via calcination, S-FIL fabrication with hybrid resins exhibits a number of other advantages over other oxide patterning techniques. These include a general reduction in the number of steps involved in surface structuring and device fabrication, lower overall process temperatures relative to direct melt embossing of oxides, and complete elimination of the need for vacuum etching for applications that do not require etching of the substrate.

A persisting challenge in developing metal−organic resins for S-FIL has been their consistently poor dispensability and low shelf life due to their susceptibility to auto-homopolymerization.[16,24] S-FIL is generally achieved by pressing a rigid, patterned template or mold into a UV-curable liquid resin to form a corresponding pattern in the resin film. Subsequently, the formed film is cured with an ultraviolet light to enable the reverse tone transfer of the mold topography into the film upon demolding. The resin is typically deposited using an inkjet dispensing unit, which is subject to clogging if the resin viscosity increases by only a few millipascal-seconds. With metal−organic hybrid resins, clogging issues are a severe challenge because auto-homopolymerization can easily generate such an increase in the resin viscosity. Thus, the resin shelf life can be as short as 2 or 3 days. More importantly, because the resin viscosity strongly influences the actual dispense volume, this instability makes it extremely difficult to achieve reproducible and predictable fabrication results in terms of film and residual layer thicknesses, control of field uniformity, and avoidance of an under-filling condition. In terms of scale-up to commercialization and large-scale expansion of nanostructures, a solution to these difficulties is crucial.

A potential solution to the problem of obtaining a more chemically stable oxide precursor was recently proposed by Dinachali et al. by reacting metal alkoxides with a polymerizable chelating agent such as 2-(methacryloyloxy)ethyl acetoacetate (MAEAA).[15] MAEAA possesses β-ketoester and methacrylate groups—the former leads to the formation of highly stable, chelated alkoxide complexes, while the latter provides the reactive group for participation in free-radical polymerization. The reaction of a metal alkoxide with MAEAA results in the formation of a metal−organic precursor mixed with an alcohol byproduct. Preliminary assessment of the suitability of these precursors was carried out by removing the alcohol byproduct under reduced pressure followed by examination to check for auto-homopolymerization. The resultant product was a stable, transparent, lightly colored, polymerizable, and viscous liquid metal oxide precursor freely soluble in acrylate-based reactive diluents with remarkable immunity to auto-homopolymerization. Resins formulated using these chelated oxide precursors exhibited at least a 30-fold improvement in shelf life relative to previously reported formulation schemes.[24] Along with enhanced performance and shelf life, in this work, we have utilized the aforementioned improved resin formulation approach to demonstrate a versatile approach for S-FIL patterning of a host of metal oxides such as Al_2O_3, HfO_2, TiO_2, ZrO_2, Nb_2O_5, and Ta_2O_5 in step-and-repeat fashion over large areas. Although patterned examples of all the oxides will be given, Nb_2O_5 in particular will be used as a representative candidate for discussing resin behavior.

RESULTS AND DISCUSSION

In general, liquid resins possess good transport properties to enable faster filling of mold cavities and the spreading of resin from areas where feature density is low to other regions where feature density is higher at low pressure (~100 kPa). S-FIL exploits these advantages in the fabrication of micro- and nanostructures in step-and-repeat fashion over an entire wafer at speeds in excess of, or competitive with, conventional techniques such as photolithography and electron beam writing, respectively. In S-FIL, a low-viscosity, photo-curable resin is locally dispensed dropwise on the substrate over a drop map area corresponding to the template patterned area. Then, a quartz template is brought into contact with the resin to form a stack. The resin is then photo-polymerized by exposing it to UV light through the transparent template, resulting in the formation of rigid imprinted features. In terms of fully organic resins, the photo-polymerizable monomers used in S-FIL are typically either acrylate- or vinyl ether-based formulations, with

the former more popular than the latter due to easy availability of inexpensive monomers.[25−29]

Most scientific activity in the field is largely confined to thermally curable resin formulations, as the monomer and precursor synthesis is relatively straightforward, and processing does not place significant restrictions on the resin properties. However, for successful S-FIL patterning of metal−organic resins, the precursor must be transparent, stable, fast curing, and of low enough viscosity to be inkjet dispensable. Furthermore, organic solvent in the resin must be kept to near-zero, as evaporation at an inkjet dispense orifice leads to condensation at the tip and this causes the alkoxide to precipitate out, leading to a white residue build-up that clogs the dispense tip orifice. These stringent requirements make metal−organic hybrid resin development for S-FIL a significant challenge.

The success of patterning functional metal oxides using S-FIL strongly depends on the resin formulation. Broadly speaking, there are four main components. First, a polymerizable metal oxide precursor, usually an inorganic coordination complex, which participates in polymerization during UV exposure and forms metal oxide after calcination of the imprinted structures. Second, a reactive diluent that is used to adjust the viscosity of the polymerizable metal−organic complex. Third, a cross-linker which provides mechanical strength, and finally fourth, a photo-initiator to initiate photo-polymerization leading to solidification of the resin. Among these four, the most critical component of the resin is the polymerizable metal oxide precursor. Such a complex should preferably be of low viscosity, transparent, resistant to auto-homopolymerization, and stable against hydrolytic activity. A popular way to form polymerizable metal−organic complexes is to react a metal alkoxide with a polymerizable monomer such as methacrylic acid or 3-butenoic acid.[16,24] This is because of the simplicity of the reaction, as metal alkoxides are very reactive compounds due to the presence of electronegative alkoxy groups that cause the metal atom to be highly prone to nucleophilic attack. Unfortunately, in most cases, the reaction between metal alkoxides with methacrylic acid[16] or 3-butenoic acid[24] does not yield a processable liquid. Furthermore, metal methacrylates, and to some extent allyl-functionalized metal complexes, suffer from a shorter shelf life due to the problem of auto-homopolymerization. Therefore, an improved reaction scheme for S-FIL resin formulation is desirable.

It has recently been reported that reacting metal alkoxides with a polymerizable chelating agent such as MAEAA yields a polymerizable metal−organic liquid that is clear, stable, flowable, and of low viscosity.[15] MAEAA is a bi-functional molecule that possesses β-ketoester and methacrylate groups. The β-ketoester group is capable of undergoing keto−enol tautomerism, as shown in eq 1; the enol form of MAEAA is stabilized by chelation with tantalum ethoxide that results in the formation of a chemically stable, chelated alkoxide perhaps due to steric hindrance (eq 2). In sol−gel chemistry, it is well-known that β-ketoester- and β-diketone-based chelating agents stabilize alkoxides and increase their long-term resistance against hydrolysis. This technique has been effectively utilized to pattern oxides using photolithography,[4,5] electron beam lithography,[6,7] two-photon lithography,[30] direct write assembly,[31] electrohydrodynamic lithography,[32] and proton beam writing.[33] In our case, the key to achieving long-term hydrolytic stability of our oxide precursors is the stabilization of alkoxides using a β-ketoester such as MAEAA, a chelating agent. We have

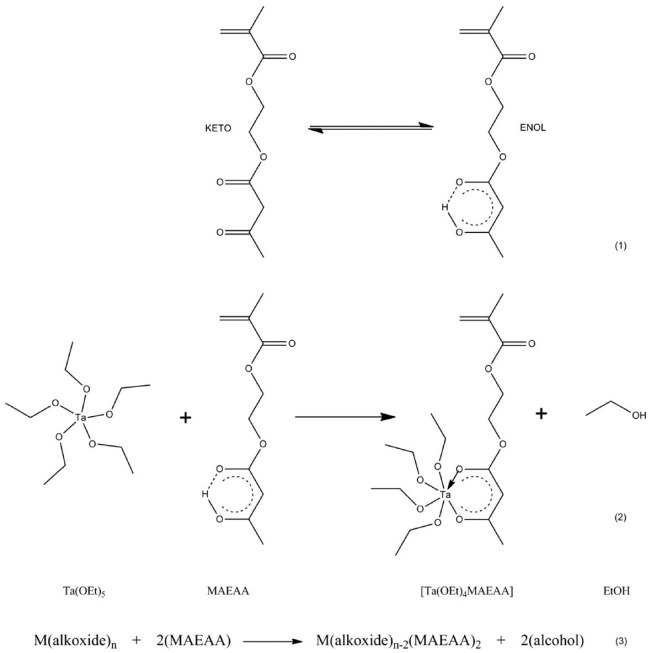

used MAEAA because it possesses β-ketoester and methacrylate groups—the former leads to the formation of highly stable, chelated alkoxide complexes, while the latter provides a reactive monomer that takes part in polymerization in the presence of a photo-initiator. The chelating reaction often results in a slight color change of the solution and yields a polymerizable metal−organic precursor.

The key condition that enables compatibility with S-FIL is in the selection of state for the candidate metal alkoxide. Only liquid-state metal alkoxides have sufficiently low viscosity at room temperature to achieve formulated resin viscosities below 20 mPa·s, the latter being an important threshold viscosity for inkjet dispensing.[27] This condition was not reported in prior works where both liquid and solid-state metal alkoxides were employed without distinction. One challenge that may arise given the state requirement would be cases where solid metal alkoxides are required as feedstock, or is the only available state for a given metal alkoxide. Further research into the feasibility of heating the metal−organic resin during inkjet dispense would be required in order to lower the viscosity to below the dispense threshold.

A further important development in enabling S-FIL processing was the elimination of organic solvents. This is contrary to common practice with purely organic resins where such solvents are used extensively for cleaning of the inkjet dispense line and dispense tip. Cleaning of our metal−organic resins leads to deposition of alkoxide residues at the tip orifice and along the dispense line upon evaporation of the solvent, leading to extensive clogging. Additionally, alcohols will generally cause the alkoxide components to precipitate out of the resin, presumably due to alcoholysis,[34] forming insoluble particles that will clog the inkjet dispense unit long after removal of the metal−organic resin. Thus, solvents were not used for cleaning the inkjet dispense unit, aside from the dispense tips which were cleaned with multiple solvents to remove all residues prior to thorough drying. This approach enabled full, automated step-and-repeat imprinting without clogging issues.

Preliminary studies were conducted to study the suitability of liquid-state metal alkoxides for S-FIL resin formulation. First,

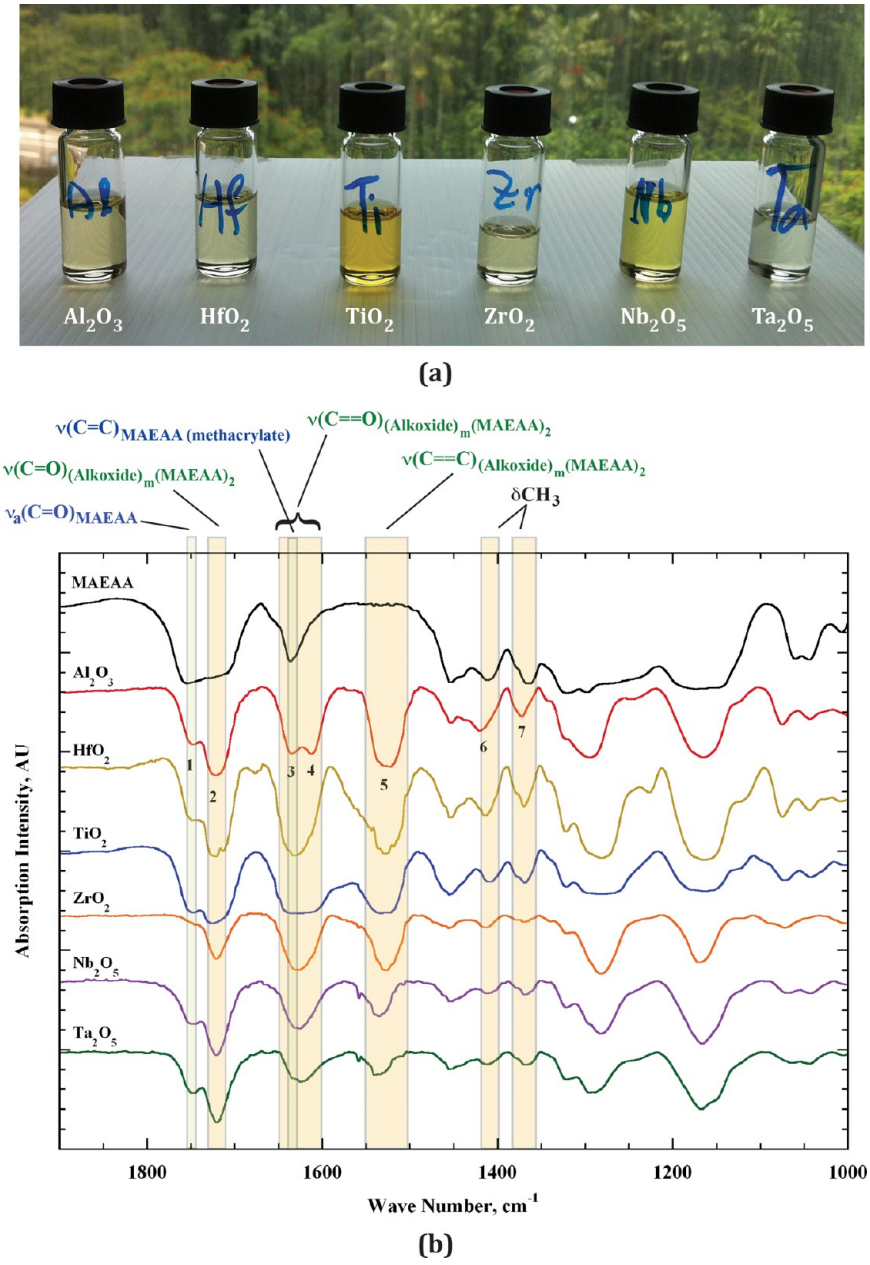

Figure 1. (a) Clear, stable, and slightly colored metal oxide precursors formed when alcohol byproduct was removed following the reaction shown in eq 3. (b) Characteristic infrared absorption peaks of metal oxide precursors formed by reacting metal alkoxide and MAEAA in a 1:2 ratio. The broad vibration bands corresponding to particular bonds are indicated at the top. Table 1 shows details of the band assignment.

various chelated metal alkoxides (of Al, Hf, Ti, Zr, Nb, and Ta) were subjected to a low pressure environment so as to remove the alcohol byproduct (eq 3). Removal of alcohol byproducts typically led to the formation of transparent, often slightly colored liquids containing polymerizable oxide precursors that were remarkably resistant to auto-homopolymerization (Figure 1a). We speculate two-fold reasons for the exceptional stability of metal alkoxides chelated with MAEAA in comparison to their corresponding methacrylic acid- and allyl-terminated carboxylic acid-chelated derivatives. Firstly, the very nature of the chelation between the metal center and the ligands is different. In the case of a carboxylic acid, the carboxylate anion replaces the alkoxy group and binds to the metal center and thus results in the final product having the same co-ordination number as the alkoxide. By contrast, when MAEAA (a β-ketoester in its enol form) is substituted for an alkoxy group, it results in the final product having an additional co-ordination number due to the extra co-ordination bond between the β-ketoester group and the metal center. Secondly, the chemical environment of the reactive end group may be reducing the occurrence of auto-homopolymerization. The longer chain length of MAEAA molecules further separates the methacrylate groups from each other due to steric hindrance. As a result, the number of collisions between the methacrylate groups is reduced, thereby decreasing the probability of auto-homopolymerization. This is in striking contrast to metal methacrylates (and to some extent allyl-functionalized metal complexes), as they undergo auto-homopolymerization upon any attempt to remove alcohol present as a byproduct from the reaction of a metal alkoxide with methacrylic acid.[16,24] We

believe that these synergistic factors contribute to the enhanced shelf life of the MAEAA-chelated metal precursors. Predictably, all the chelated precursors, except for ZrO_2, showed excellent stability over a storage period of more than 3 months at room temperature. They were found to be transparent and flowable. The storage period for ZrO_2 was found to be limited to ~2 weeks.

Table 1. Characteristic Infrared Absorption Peaks of Chelated Metal Oxide Precursors[a]

absorption peak (cm^{-1})	assignment	peak number
1746	ν_a(C═O)	1
1721	ν(C═O)	2
1634	ν(C═C)	3
1609	ν(C⎓O)	4
1522	ν(C⎓C)	5
1418, 1372	δCH_3	6, 7

[a]The principal peaks indicated below are for the Al_2O_3 precursor. Other chelated precursors show similar values, as shown in Figure 1b.

To understand the chelation reaction, FTIR spectroscopy was used to characterize the viscous polymerizable metal oxide precursors (Figure 1b). Their FTIR spectra were found to be similar and show a large number of absorption bands/peaks between 1000 and 1800 cm^{-1}. The pair of absorption peaks corresponding to the ν(C⎓C) and ν(C⎓O) vibrations of the chelate ring at 1522 and 1609 cm^{-1}, respectively, is attributed to the bidentate character of cation-bonded MAEAA. This is indicative of the formation of the chelated complex.[35,36] Noteworthy is the presence of characteristic peaks of the carbonyl group at 1721 cm^{-1} and the methacrylate double bond at 1634 cm^{-1} in MAEAA-functionalized metal oxide precursors; the latter strongly suggests the preservation of a polymerizable double bond in the complex. A shoulder at 1746 cm^{-1} that corresponds to the carbonyl group of MAEAA may indicate incomplete reaction between MAEAA and the corresponding metal alkoxides (Figure 1b).[36]

Resins for the S-FIL of oxides were formulated by adding reactive diluent, cross-linker, and photo-initiator to the respective polymerizable metal oxide precursors. Since the precursors have a relatively high viscosity, *iso*-butyl acrylate, a reactive diluent, was added to lower the viscosity. Ethylene glycol diacrylate served as a cross-linker, and due to its relatively low viscosity, it also partly served the purpose of a reactive diluent. The molar ratio between alkoxide, MAEAA, *iso*-butyl acrylate, and ethylene glycol diacrylate was 1:2:2:1 for Al_2O_3, HfO_2, TiO_2, and ZrO_2 resins. On the other hand, Ta_2O_5 and Nb_2O_5 resins had a ratio of 1:2:1:1. Additional *iso*-butyl acrylate was added to the former set of resins due to the relatively high viscosity of their oxide precursors. Of course, it is worthwhile to note that reducing the viscosity in this manner comes at the cost of additional shrinkage and loss of oxide content upon calcination. The formulation of the above-mentioned molar ratios takes this consideration into mind in order to maintain post-calcination integrity. The final resin composition in all cases possessed a viscosity of <10 mPa·s. For comparison, Nb_2O_5 resin and a fully organic "blank" formulation in a 2:1:1 molar ratio of MAEAA, *iso*-butyl acrylate, and ethylene glycol diacrylate exhibited viscosities of 7.5 and 4.6 mPa·s, respectively. These resin formulations were found to possess excellent dispensability with viscosities well within the suggested limit of 20 mPa·s.[27]

To determine the absorbance of UV radiation by the oxide resins, ultraviolet-visible (UV-vis) spectrophotometry was carried out (Figure 2a). It was seen that Al_2O_3, HfO_2, ZrO_2,

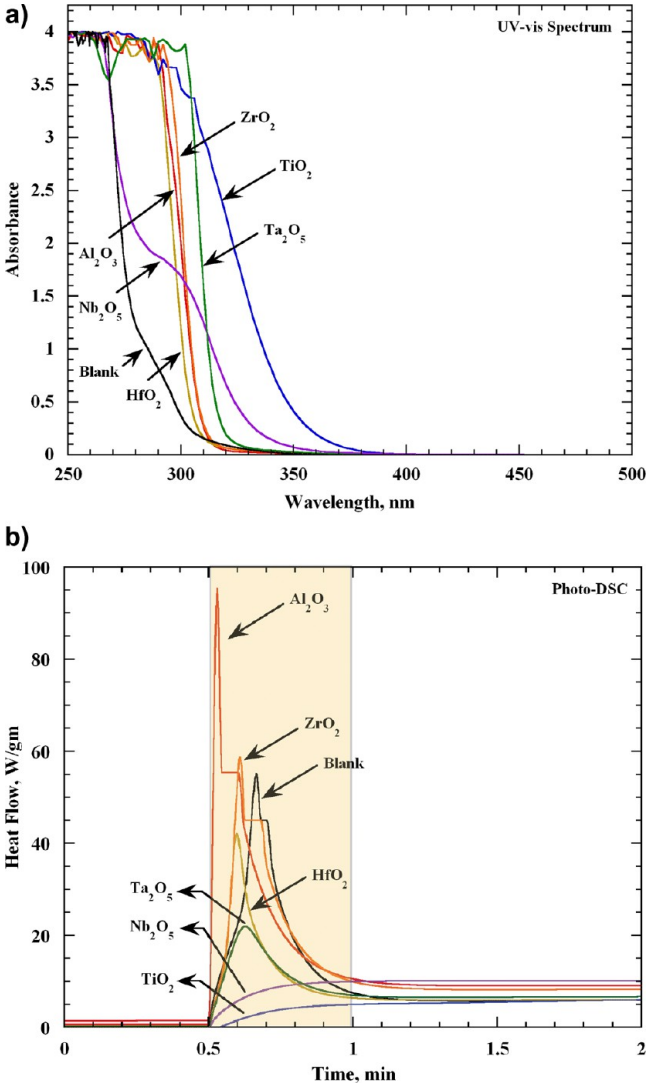

Figure 2. (a) UV-vis spectroscopy and (b) photo-DSC of Al_2O_3, HfO_2, TiO_2, ZrO_2, Nb_2O_5, Ta_2O_5, and "blank" (fully organic) resins.

and Ta_2O_5 resins have a steep and sharp UV absorption starting at ~320 nm unlike TiO_2 and Nb_2O_5 resins which show a wider range of wavelengths for UV absorption. Photo-DSC studies showed that it takes about 30 s to completely cure each resin with UV exposure (Figure 2b). Figure 3 shows how individual resin components contribute to the final FTIR spectrum of Nb_2O_5 resin, where said spectrum is generally representative of all oxide resins presented here. The effect of UV radiation on Nb_2O_5 resin was also followed by FTIR. After a 2 min UV exposure in air, the —C═C peak disappears, confirming that the resin completely cures after this period of exposure. Furthermore, it was observed that the metal−carbonyl chelation bond remains unaffected during the polymerization, implying that the metal atoms are incorporated into the polymerized network. This, of course, confirms that resins containing oxide precursors will calcine into oxide nanostructures after the S-FIL patterning step.

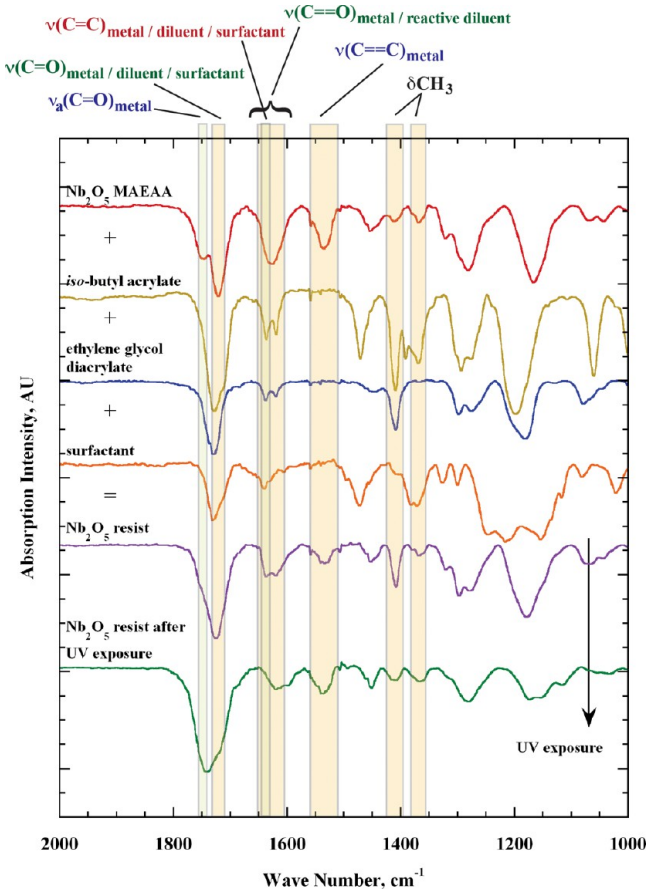

Figure 3. FTIR spectra of individual components contributing to the final FTIR spectrum of Nb_2O_5 resin. At the bottom are the pre- and post-UV exposure spectra of Nb_2O_5 resin showing the effect of photopolymerization. Note the absence of the —C═C band after exposure.

A Molecular Imprints Imprio 100 unit (Molecular Imprints, Inc.) was used for S-FIL patterning of our metal oxide resins. A schematic of the process steps is shown in Figure 4, where the resin was first deposited on a silicon wafer by direct drop-dispensing, followed by contact and spreading by a quartz template containing a 100 nm line and space grating, with an aspect ratio of 1. The volume of individual droplets was pre-adjusted during trial runs in order to achieve fully patterned imprint fields (see the Supporting Information). Dispense tips were thoroughly cleaned in an ultrasonic bath sequence of methanol, ethanol, and *iso*-propyl alcohol and then completely dried with a nitrogen gas gun in order to remove both alkoxide residues and solvents. After contact and spreading of the resin, photo-curing was accomplished via mercury-arc lamp UV irradiation through the transparent quartz template for 60 s. Separation forces were found to be in the range 10−25 N for different oxide resins for a 1 cm^2 patterned field. Full step-and-repeat mode is demonstrated in Figure 5a using Nb_2O_5 resin, where a total of nine fields were imprinted across a 4 in. silicon wafer. Figures 5b and 6 show SEM cross section and overhead views of as-imprinted 100 nm gratings as well as the calcined results for Nb_2O_5, Al_2O_3, HfO_2, TiO_2, ZrO_2, and Ta_2O_5 resins.

Due to similar patterning behavior, Nb_2O_5 resin will be discussed here in greater detail. Figure 5b shows the top view and cross-sectional SEM images of imprinted Nb_2O_5 resin. The cross-sectional SEM image shows that the width and height of the as-imprinted features were slightly smaller than the actual dimensions of the mold, a result attributed to shrinkage inherent to acrylic resins.[37] For example, 100 nm grating molds gave ∼76 nm line-widths with a residual layer thickness of ∼80 nm. Despite shrinkage, the aspect ratio of the mold was closely maintained. Likewise, similar observations can be made from the gratings patterned with Al_2O_3, HfO_2, TiO_2, ZrO_2, and Ta_2O_5 resins (Figure 6 and Table 2).

The calcination step involves decomposition and removal of organic content from the polymerized resins, followed by sintering to form a solid oxide. Sintering is a process of densification driven by interfacial energy. The atoms in formed metal-oxide migrate by diffusion in such a way as to eliminate porosity, thereby reducing the solid−air interfacial area and increasing the oxide density. Holding the sintered material at a high enough temperature can lead to the formation of nanocrystalline oxide grains and subsequently their growth via Ostwald ripening.[38] TGA analysis was used to determine the minimum temperature required to remove the organic content completely during calcination to form nanostructured oxide films. It was noted that an isothermal calcination at 475 °C for 1 h in air was sufficient to burn off organic content from all candidate resins (Figure 7), and in some cases, the heat treatment was sufficient to form a crystalline phase in the oxide film as well (see the Supporting Information). This calcination step was used to convert the structured metal−organic films to their respective oxides. However, such low temperature heat-treatment is bound to leave behind small amounts of carbonaceous impurity in oxides. SEM and AFM analyses were used to study the effect of calcination on the pattern shrinkage (Figure 5b, Figure 6, and Table 2). The final size of oxide lines was found to be in a range of 20−25 nm. AFM analysis showed that an aspect ratio of 1 (of the mold) was closely maintained by all the patterned oxides. This suggests that the shrinkage is nearly uniform over the entire imprinted area. Feature shrinkage depends on the amount of the oxidized metal in relation to the total amount of the oxide precursor, the volume of other organic components such as reactive diluents, cross-linkers and additives, the calcination temperature, and finally the size of the oxide unit cell formed after calcination. In general, however, calcination shrinkage does tend to introduce sidewall tapering to the oxide structures, as the top surface of oxide features is a free surface while the feature base is not, though the feature base and the residual layer all shrink together, which mitigates the tapering effect. The degree of feature tapering depends on the degree of calcination shrinkage and the thickness of the residual layer (a very thin residual layer will lead to substrate pinning effects that inhibit lateral shrinkage of the residual layer and, in turn, the feature base).

S-FIL patterning was also carried out with more arbitrary mold structures, as shown in Figure 5c with Nb_2O_5 resin. A quartz template containing composite features such as hexagonal dots, micrometer-scale lines, nanoscale lines with different pattern densities, and a mixture of micro- and nanoscale features was employed as a general test of the filling and transport performance of Nb_2O_5 resin (Figure 5c). Despite the variation in pattern geometry and density, the mold filling behavior of the resin was found to be comparable to fully organic acrylic resins. Obtained yield of early imprint fields was estimated by inspection to be >95%. However, after approximately five fields were successfully patterned, a decrease in the patterned area was observed due to caking onto the quartz mold. This is most likely due to progressive degradation of the silanized anti-stick coating applied to the mold.[39]

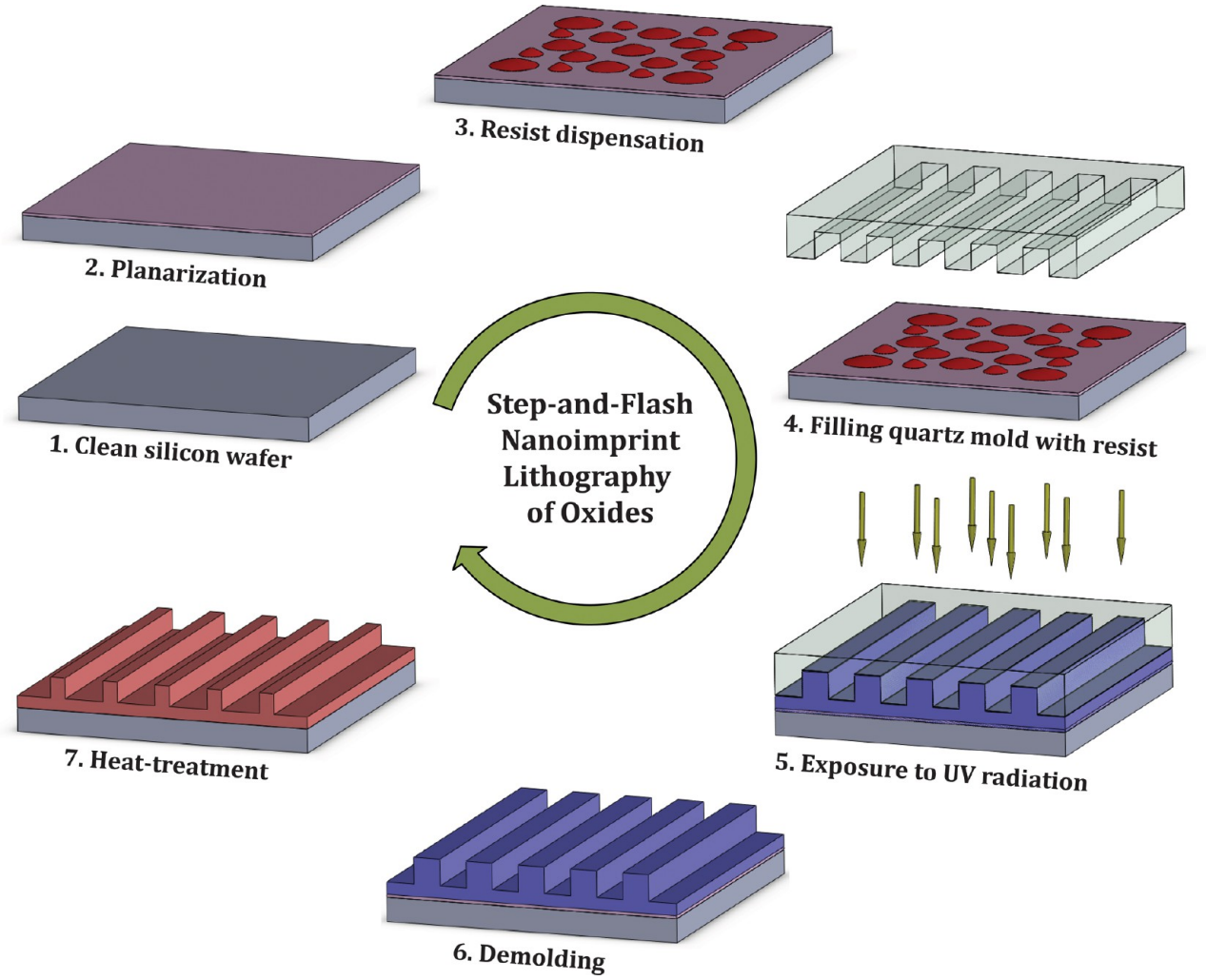

Figure 4. Schematic representation of the process steps involved in S-FIL patterning and calcination of oxide films.

CONCLUSIONS

To conclude, we have demonstrated a versatile route for S-FIL nanostructuring of a host of oxide films including Al_2O_3, HfO_2, TiO_2, ZrO_2, Ta_2O_5, and Nb_2O_5 over a large area using S-FIL. This route is instrumental in facilitating easy access to arbitrary nanoscale oxide structures via calcination shrinkage, with long shelf life formulations that are chemically stable, dispensable, and amenable to scale-up. The route was achieved by reacting liquid-state metal alkoxides with MAEAA, a polymerizable chelating agent, and mixing them with a reactive diluent, cross-linker, and photo-initiator. MAEAA uses the synergistic effect of β-ketoester and methacrylate groups to achieve excellent chemical stability and fast curing of the metal oxide precursor, respectively. The excellent resistance to auto-homopolymerization exhibited by these polymerizable metal oxide precursors allows for extension of shelf life to at least 3 months without clogging of the inkjet dispense unit. With the enhanced stability in viscosity, it is expected that further dispense recipe optimizations will allow for uniform dispense volumes and, in turn, uniform residual layers in addition to full-field patterning as demonstrated herein. Additionally, the β-ketoester group in MEAA also enables sol−gel processing and complex formation with a large variety of alkoxides with a single formulation scheme, which is not possible with allyl-functionalized metal complexes or metal methacrylate-based monomers. Given the advantages of a sol−gel route and the associated stability it provides to the alkoxide complex, we believe this approach is versatile enough to enable formulation and S-FIL patterning of many other oxides in addition to those shown herein. This flexibility is very important to facilitate commercial adoption. Finally, unlike allyl-functionalized metal complexes, polymerizable oxide precursors are near-transparent, leading to less absorption of irradiated UV light during S-FIL patterning and consequently shorter exposure times and higher throughput.

Calcination of various metal−organic resin films imprinted with a 100 nm line and space mold enabled linewidths, with shrinkage, in a narrow range of 20−25 nm. This method of rapid patterning of oxide films using S-FIL can potentially decrease the number of steps involved in surface structuring and device fabrication, lower the overall process temperatures needed to achieve patterned oxide films in comparison to direct melt embossing of oxides, and eliminate the need for vacuum etching for devices that do not require etching of the substrate.

EXPERIMENTAL SECTION

Materials. Aluminium (III) tri-*sec*-butoxide (97%, Sigma Aldrich), hafnium (IV) *tert*-butoxide (99.9%, Alfa Aesar), titanium (IV) ethoxide (Sigma Aldrich), zirconium (IV) *tert*-butoxide (99%, Strem Chemicals), niobium (V) ethoxide (99.95%, Sigma Aldrich), tantalum (V) ethoxide (99.98%, Sigma Aldrich), and 2-(methacryloyloxy)ethyl acetoacetate (95%, Sigma Aldrich) were used as received. Ethylene

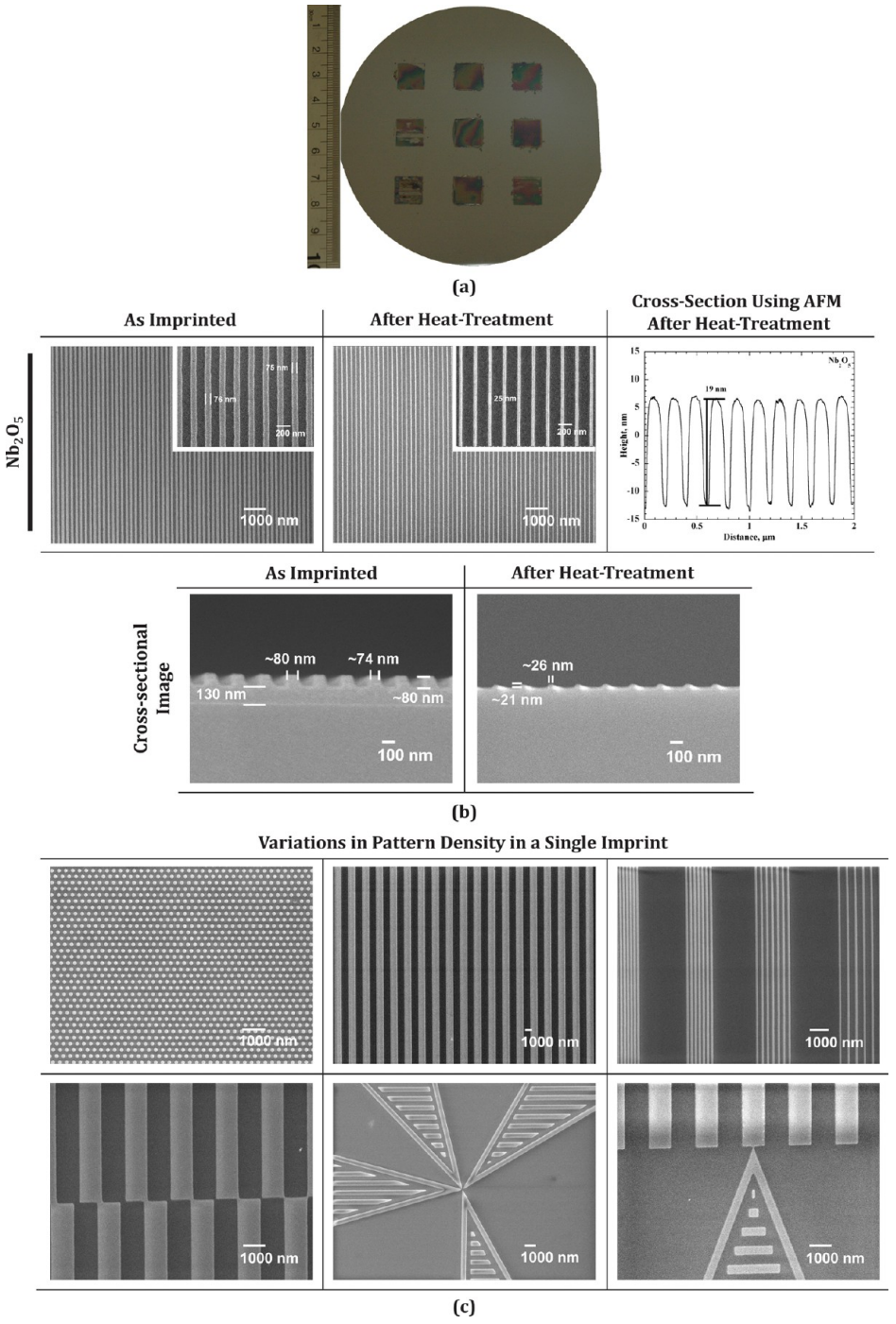

Figure 5. (a) Demonstration of step-and-repeat S-FIL patterning of nine imprint fields across a 4 in. silicon wafer at high yield using Nb_2O_5 resin with a quartz template, the latter consisting of 100 nm line/space gratings over a 1 cm × 1 cm area. Each field was imprinted in a serpentine sequence starting from the top right and moving down. (b) Composite SEM images of as-imprinted, calcined Nb_2O_5 gratings. The insets show the gratings at higher magnification. At the right is a corresponding AFM line trace of the imprinted, calcined structures. At the bottom are cross-sectional SEM images of the gratings before and after calcination. (c) Immunity to the effect of variation in pattern density in a mold during an imprint. From top left, clockwise: SEM images of 150 nm dot pattern, with 150 nm edge-to-edge spacing; 1 μm lines with 1 μm spacing; 100 nm lines with 50, 100, 150, and 300 nm edge-to-edge spacing; a composite pattern with micrometer and nanoscale features; triangles with micrometer scale thicknesses converging with nanoscale spacing between them; micrometer-sized lines showing a vernier scale.

glycol diacrylate (Sigma Aldrich), *iso*-butyl acrylate (Sigma Aldrich), 3,3,4,4,5,5,6,6,7,7,8,8,9,9,10,10,10-heptadecafluorodecyl methacrylate (Sigma Aldrich), and 2-hydroxy-2-methylpropiophenone (Sigma Aldrich) were used without any further purification.

Resin Formulation and Characterization. The alkoxides of aluminium, hafnium, titanium, zirconium, niobium, and tantalum were reacted with MAEAA in a 1:2 molar ratio inside a glove box (<5% relative humidity), leading to the formation of a chelated precursor and an alcohol as a byproduct. The byproduct was preferentially removed by subjecting the mixture to a reduced pressure in a vacuum chamber. In all cases, a viscous liquid was obtained. To this, *iso*-butyl acrylate and ethylene glycol diacrylate were added as reactive diluent and cross-linker, respectively. To reduce the surface energy of imprinted resin and enable clean demolding after S-FIL patterning,

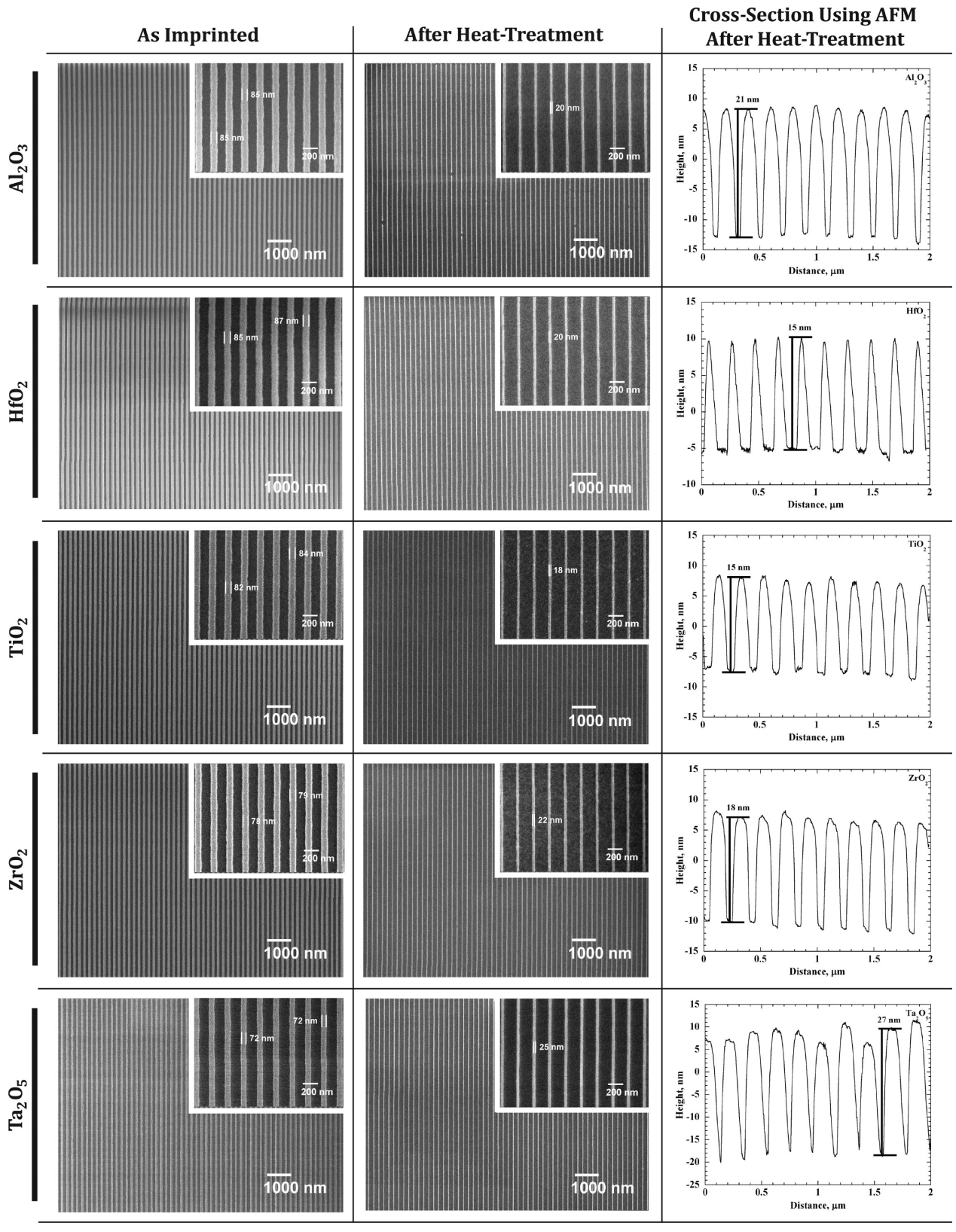

Figure 6. Composite SEM images of various imprinted, calcined structures of Al_2O_3, HfO_2, TiO_2, ZrO_2, and Ta_2O_5 using a 100 nm line and space grating quartz template. The insets show the structures at a higher magnification. The corresponding AFM line traces are shown at the right.

2 wt % 3,3,4,4,5,5,6,6,7,7,8,8,9,9,10,10,10-heptadecafluorodecyl methacrylate was added to the resin formulation as a surfactant, along with 2 wt % 2-hydroxy-2-methylpropiophenone as a photo-initiator. Finally, the resins (henceforth called "oxide resins" and more specifically, e.g., "Nb_2O_5 resin") were purged with argon gas for 4−6 min to reduce the concentration of dissolved O_2 and thereby reduce oxygen inhibition.

A Nicolet 6700 Fourier transform infrared (FTIR) spectroscope was used to analyze the change in molecular structure of chelated precursors and of the resins before and after photopolymerization. The

Table 2. Summary of the Approximate Feature Size Reduction at Every Step of the Imprinting Process of Various Oxides with a 100 nm Line and Space Grating Mold (Aspect Ratio 1)[a]

	feature size of the imprint after S-FIL		oxide feature size after the heat-treatment of imprinted structures		
resin	width of imprint (nm)	feature size reduction (%)	width of the oxide feature (nm)	feature size reduction (%)	total feature size reduction with respect to mold feature size (%)
Al_2O_3	85	15%	20	76%	80%
HfO_2	86	14%	20	77%	80%
TiO_2	83	17%	18	78%	82%
ZrO_2	79	21%	22	72%	78%
Nb_2O_5	76	24%	25	68%	75%
Ta_2O_5	72	21%	25	65%	75%

[a]The imprinted patterns were subjected to an isothermal calcination at 475 °C for 1 h.

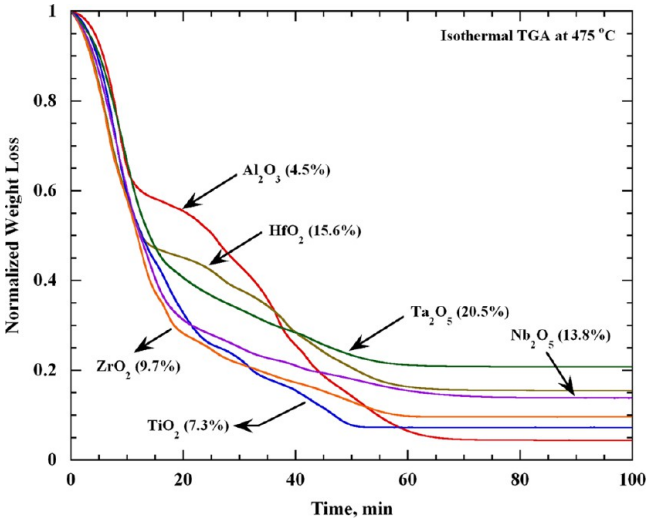

Figure 7. Isothermal TGA analysis at 475 °C of Al_2O_3, HfO_2, TiO_2, ZrO_2, Nb_2O_5, and Ta_2O_5 resins.

degradation temperature of organic constituents and formation of metal oxides was studied using thermogravimetric analysis (TA Instruments Q500). A photodifferential scanning calorimeter (p-DSC, TA Instruments Q100) equipped with a UV source (power: 300 mW cm^{-2}) was used to estimate the curing time for different resins.

Step-and-Flash Imprint Lithography of Oxides. An Imprio 100 from Molecular Imprints, Inc. (USA), was used to carry out step-and-flash imprint lithography of oxides. Double-sided, polished 4 in. silicon wafers were used as substrates. Silicon wafers and quartz templates were cleaned using piranha solution (3:7 by volume of 30% H_2O_2 and H_2SO_4, 200 °C) for 1 h to remove surface organic contaminants. This was followed by washing with deionized water and blow-drying using a nitrogen gas gun. After cleaning, the silicon wafers were spin-coated with a 2 nm thin layer of adhesion promoter called TranSpin (Molecular Imprints, Inc.) and baked at 195 °C for 5 min. Pre-cleaned quartz templates containing the various features presented herein were silanized with 1*H*,1*H*,2*H*,2*H*-perfluorodecyltrichlorosilane for 8 h to decrease their surface energy and to enable clean separation after imprinting. The Imprio 100 utilizes a single orifice drop dispense tip and dispenses resin droplets according to a computer generated drop map. A suitable drop map was programmed according to the features present on the quartz template. The silicon wafer and quartz template were then loaded and precision-leveled against each other. S-FIL patterning was conducted by bringing the wafer and template into contact in the presence of a helium shroud. Resin spreading was accomplished under an applied force of 8 N for 180 s, followed by exposure of the stack to broadband UV irradiation for 60 s at an intensity of ~4.4 mW cm^{-2}. Finally, vertical separation of the cured, patterned field was accomplished by applying a tensile load within a range of 100−250 kPa. This process is repeated, *sans* leveling, to step-and-repeat imprint fields across the wafer.

For post-S-FIL cleaning of quartz mold, the piranha solution was found to work well to remove metal−organic hybrid resin residues from the surface, as long as no other processing was carried out on the mold after the cured resin was caked onto the mold. Destruction of the organic component of the resin was generally sufficient to ensure complete removal.

Characterization of Imprint Results. To study the topography and morphology of imprinted features before and after calcination, scanning electron and atomic force microscopy were used. A JEOL JSM6700F field-emission scanning electron microscope (FE-SEM) was used to acquire high-resolution images. A Digital Instruments Nanoscope IV atomic force microscope (AFM) was used to find the height of the nanostructures. For X-ray diffraction (XRD) analysis, the oxide resins presented herein were spin-coated on a silicon substrate, photo-polymerized with UV radiation, and finally calcined at different temperatures. A Bruker D8 general area detector diffraction system (GADDS) equipped with a Cu Kα source was used for XRD analysis of the metal oxide films.

■ ASSOCIATED CONTENT

Ⓢ Supporting Information

Droplet optimization in step-and-flash nanoimprint lithography using oxide resins; quartz mold used for step-and-flash imprint lithography; X-ray diffraction results; calcination of metal−organic hybrid resins; estimate of average grain size from X-ray diffraction data; optical and electrical properties of calcined TiO_2; XPS study of the presence of residual fluorine in calcined Nb_2O_5. This material is available free of charge via the Internet at http://pubs.acs.org.

■ AUTHOR INFORMATION

Corresponding Authors

*E-mail: j-dumond@imre.a-star.edu.sg.
*E-mail: saifullahm@imre.a-star.edu.sg.

Notes

The authors declare no competing financial interest.

■ ACKNOWLEDGMENTS

S.S.D. gratefully acknowledges the A*STAR Graduate Academy (A*GA) for providing him the A*STAR Graduate Scholarship for his Ph.D. study. Assistance of Ms. Ice Tee in UV-vis spectroscopy is gratefully acknowledged. This work was partially supported by the A*STAR-JST Project No. IMRE/12-2P0802 and the A*STAR Nanoimprint Foundry Project No. IMRE/13-2B0278.

■ REFERENCES

(1) Patzke, G. R.; Zhou, Y.; Kontic, R.; Conrad, F. *Angew. Chem., Int. Ed.* **2011**, *50*, 826−859.
(2) Reiner, J. W.; Kolpak, A. M.; Segal, Y.; Garrity, K. F.; Ismail-Beigi, S.; Ahn, C. H.; Walker, F. J. *Adv. Mater.* **2010**, *22*, 2919−2938.
(3) Kamiya, T.; H. Hosono, H. *NPG Asia Mater.* **2010**, *2*, 15−22.
(4) Tohge, N.; Shinmou, K.; Minami, T. *J. Sol-Gel Sci. Technol.* **2000**, *19*, 119−123.
(5) Tohge, N.; Shinmou, K.; Minami, T. *J. Sol-Gel Sci. Technol.* **1994**, *2*, 581−585.
(6) Saifullah, M. S. M.; Subramanian, K. R. V.; Tapley, E.; Kang, D. -J.; Welland, M. E.; Butler, M. *Nano Lett.* **2003**, *3*, 1587−1591.

(7) Subramanian, K. R. V.; Saifullah, M. S. M.; Tapley, E.; Kang, D. -J.; Welland, M. E.; Butler, M. *Nanotechnology* **2004**, *15*, 158−162.
(8) Saifullah, M. S. M.; Subramanian, K. R. V.; Kang, D. -J.; Anderson, D.; Huck, W. T. S.; Jones, G. A. C.; Welland, M. E. *Adv. Mater.* **2005**, *17*, 1757−1761.
(9) Koshida, N.; Ohtaka, K.; Ando, M.; Komuro, M.; Atoda, N. *Jpn. J. Appl. Phys.* **1989**, *28*, 2090−2094.
(10) Schrift, H. *J. Vac. Sci. Technol., B* **2008**, *26*, 458−480.
(11) Costner, E. A.; Lin, M. W.; Jen, W.-L.; Willson, C. G. *Annu. Rev. Mater. Res.* **2009**, *39*, 155−180.
(12) Guo, L. J. *Adv. Mater.* **2007**, *19*, 495−513.
(13) Dumond, J. J.; Low, H. Y. *J. Vac. Sci. Technol., B* **2012**, *30*, 010801.
(14) Byeon, K. -J.; Lee, H. *Eur. Phys. J.: Appl. Phys.* **2012**, *59*, 10001.
(15) Dinachali, S. S.; Saifullah, M. S. M.; Ganesan, R.; Thian, E. S.; He, C. *Adv. Funct. Mater.* **2013**, *23*, 2201−2211.
(16) Ganesan, R.; Lim, S. H.; Saifullah, M. S. M.; Hussain, H.; Kwok, J. X. Q.; Tse, R. L. X.; Bo, H. A. P.; Low, H. Y. *J. Mater. Chem.* **2011**, *21*, 4484−4492.
(17) Matsui, S.; Igaku, Y.; Ishigaki, H.; Fujita, J.; Ishida, M.; Ochiai, Y.; Namatsu, H.; Komuro, M. *J. Vac. Sci. Technol., B* **2003**, *21*, 688−692.
(18) Kwon, S. J.; Park, J. H.; Park, J. G. *J. Electroceram.* **2006**, *17*, 455−459.
(19) Hampton, M. J.; Williams, S. S.; Zhou, Z.; Nunes, J.; Ko, D. H.; Templeton, J. L.; Samulski, E. T.; DeSimone, J. M. *Adv. Mater.* **2008**, *20*, 2667−2673.
(20) Yang, K.-Y.; Yoon, K.-M.; Choi, K. W.; Lee, H. *Microelectron. Eng.* **2009**, *86*, 2228−2231.
(21) Yang, K.-Y.; Yoon, K.-M.; Lim, S.; Lee, H. *J. Vac. Sci. Technol., B* **2009**, *27*, 2786−2789.
(22) Radha, B.; Lim, S. H.; Saifullah, M. S. M.; Kulkarni, G. U. *Sci. Rep.* **2013**, *3*, 1078.
(23) Raut, H. K.; Dinachali, S. S.; He, A. Y.; Ganesh, V. A.; Saifullah, M. S. M.; Law, J.; Ramakrishna, S. *Energy Environ. Sci.* **2013**, *6*, 1929−1937.
(24) Ganesan, R.; Dumond, J.; Saifullah, M. S. M.; Lim, S. H.; Hussain, H.; Low, H. Y. *ACS Nano* **2012**, *6*, 1494−1502.
(25) Long, B. K.; Keitz, B. K.; Willson, C. G. *J. Mater. Chem.* **2007**, *17*, 3575−3580.
(26) Kim, E. K.; Stacey, N. A.; Smith, B. J.; Dickey, M. D.; Johnson, S. C.; Trinque, B. C.; Willson, C. G. *J. Vac. Sci. Technol., B* **2004**, *22*, 131−135.
(27) Palmieri, F.; Adams, J.; Long, B.; Heath, W.; Tsiartas, P.; Willson, C. G. *ACS Nano* **2007**, *1*, 307−312.
(28) Heath, W. H.; Palmieri, F.; Adams, J. R.; Long, B. K.; Chute, J.; Holcombe, T. W.; Zieren, S.; Truitt, M. J.; White, J. L.; Willson, C. G. *Macromolecules* **2008**, *41*, 719−726.
(29) Takei, S. *Jpn. J. Appl. Phys.* **2010**, *49*, 071602.
(30) Passinger, S.; Saifullah, M. S. M.; Reinhardt, C.; Subramanian, K. R. V.; Chichkov, B. N.; Welland, M. E. *Adv. Mater.* **2007**, *19*, 1218−1221.
(31) Duoss, E. B.; Twardowski, M.; Lewis, J. A. *Adv. Mater.* **2007**, *19*, 3485−3489.
(32) Voicu, N. E.; Saifullah, M. S. M.; Subramanian, K. R. V.; Welland, M. E.; Steiner, U. *Soft Matter* **2007**, *3*, 554−557.
(33) Van Kan, J. A.; Bettiol, A. A.; Chiam, S. Y.; Saifullah, M. S. M.; Subramanian, K. R. V.; Welland, M. E.; Watt, F. *Nucl. Instrum. Methods Phys. Res., Sect. B* **2007**, *260*, 460−463.
(34) Bradley, D. C.; Mehrotra, R. C.; Gaur, D. P. *Metal Alkoxides*; Academic Press: London, 1986.
(35) Méndez-Vivar, J.; Bosch, P.; Lara, V. H.; Mendoza-Serna, R. *J. Sol-Gel Sci. Technol.* **2002**, *25*, 249−254.
(36) Miele-Pajot, N.; Hubert-Pfalzgraf, L. G.; Papiernik, R.; Vaissermann, J.; Collier, R. *J. Mater. Chem.* **1999**, *9*, 3027−3033.
(37) Patel, M. P.; Braden, M.; Davy, K. W. *Biomaterials* **1987**, *8*, 53−56.
(38) Brinker, C. J.; Scherer, G. W. *Sol-Gel Science - The Physics And Chemistry Of Sol-Gel Processing*; Academic Press, Inc.: San Diego, CA, 1990.
(39) Truffier-Boutry, D.; Zelsmann, M.; De Girolamo, J.; Boussey, J.; Lombard, C.; Pépin-Donat, B. *Appl. Phys. Lett.* **2009**, *94*, 044110.